

Goal-Oriented Error Estimation for the Automatic Variationally Stable FE Method for Convection-Dominated Diffusion Problems

Eirik Valseth^{a,*}, Albert Romkes^b

^a*Oden Institute for Computational Engineering and Sciences, The University of Texas at Austin, Austin, TX 78712, USA*

^b*Department of Mechanical Engineering, South Dakota School of Mines & Technology, 501 E. St. Joseph Street, Rapid City, SD 57701, USA*

Abstract

We present goal-oriented *a posteriori* error estimates for the automatic variationally stable finite element (AVS-FE) method [1] for scalar-valued convection-diffusion problems. The AVS-FE method is a Petrov-Galerkin method in which the test space is broken, whereas the trial space consists of classical FE basis functions, e.g., C^0 or Raviart-Thomas functions. We employ the concept of optimal test functions of the discontinuous Petrov-Galerkin (DPG) method by Demkowicz and Gopalakrishnan [2–6], leading to unconditionally stable FE approximations. Remarkably, by using C^0 or Raviart-Thomas trial spaces, the optimal discontinuous test functions can be computed in a completely decoupled element-by-element fashion.

To establish the error estimators we present two approaches: *i*) following the classical approach of Becker and Rannacher [7], i.e., the dual solution is sought in the (broken) test space, and *ii*) introducing an alternative approach in which we seek C^0 , or Raviart-Thomas, AVS-FE approximations of the dual solution by using the underlying strong form of the dual boundary value problem (BVP). Various numerical verifications for 2D convection-dominated diffusion BVPs show that the estimates of the approximation error by the new alternative method are highly accurate, while the classical approach leads to error estimates of poor quality. Lastly, we present an algorithm for

*Corresponding author

Email addresses: Eirik@utexas.edu (Eirik Valseth), Albert.Romkes@sdsmt.edu (Albert Romkes)

h -adaptive processes based on control of the numerical approximation error via the new alternative approach. Numerical verifications show that the estimator maintains high accuracy as the error converges to zero.

Keywords: discontinuous Petrov-Galerkin methods, *a posteriori* error estimation, and convection-diffusion problems

2000 MSC: 65N30 65N12

1. Introduction

In adaptive mesh refinement algorithms, *a posteriori* error estimation [8, 9] is needed to provide quantified assessments of the numerical approximation error, as well as error indicators to guide the adaptive process. Residual-based goal-oriented error estimates have been developed for multiple applications and FE methods, e.g. see [7, 10–13]. It involves the solution of a dual problem, which for Bubnov-Galerkin and Petrov-Galerkin methods [14–18] suffers from the same numerical instabilities as the primal problem in the presence of convection. Thus, the FE meshes for the dual problem have to be refined so as to adequately capture any boundary or internal layers and thereby avoid any numerical instabilities. It makes the classical methods unsuitable for goal-oriented error estimation for this class of problems.

However, goal-oriented error estimates have been successfully applied to conditionally stable FE methods by several authors for convection-diffusion problems [19–23]. In these works, stabilization schemes such as the streamlined-upwind Petrov-Galerkin (SUPG) [24] method are used to stabilize both the primal and dual problems. The reported effectivity of the estimates varies based on the stabilization chosen, type of error to be estimated (approximation vs. modeling), and the Quantity of interest (QoI) used. In [21, 23], Schwegler *et al.* explicitly investigate the stabilization of the dual problem and its influence on the estimate. Stabilized discontinuous Galerkin (DG) methods have also been applied to goal-oriented error estimates for convection-diffusion problems with success, we refer to [25] and references therein. While these error estimation efforts have been successful, the conditionally stable nature of the methods do require a priori analyses to properly establish the parameters needed to achieve stability which

can be extremely arduous and have to be done on a problem-by-problem basis.

Unconditionally stable FE methods such as the least squares FE method (LSFEM) [26] and the DPG method [2–6] resolve the issue of conditional numerical instability. However, these methods generally use a built-in *a posteriori* error estimator based on the error in the energy norm induced by its bilinear form to drive adaptivity (see, e.g., [3, 6, 27, 28]). The simplicity and quality of this type of estimator make it the most commonly employed for residual minimization techniques such as the DPG method and LSFEM. In [29], Keith *et al.* introduce the concept of goal-oriented adaptive mesh refinement for the DPG method. However, their goal is not so much to estimate the errors in FE computations but rather the introduction of a new duality theory that is used as a vessel for new adaptive mesh refinement strategies. In [30], the least squares functional is modified by adding terms incorporating QoIs to enhance the quality of the built-in estimator used to drive the adaptive mesh refinement. A similar approach is taken by Cai, Ku *et al.* in [31–33] to both estimate errors and drive mesh refinements.

While the error estimation in the aforementioned references has been successful, the stabilization efforts required can be arduous by demanding in-depth a priori error analyses on a problem-by-problem basis. In addition, to our best knowledge there are no published results for the DPG method that state the effectivity of goal-oriented *a posteriori* error estimates for convection-diffusion problems. Goal-oriented error estimation in the LSFEM for convection-dominated diffusion problems is less attractive due to the highly diffusive nature of its FE approximations for coarse meshes which can lead to estimates with poor accuracy. Our goal is therefore to introduce a new framework for the goal-oriented *a posteriori* error estimation for the automatically stable AVS-FE method that delivers highly accurate predictions of the error in user defined QoIs.

The AVS-FE method introduced by Calo, Romkes and Valseth [1] provides a functional setting to analyze singularly perturbed problems, such as convection-dominated diffusion. The AVS-FE method is a hybrid between the DPG method [2–6] and the classical mixed FE methods in the sense that the trial space consists of globally continuous functions, while the test space consists of piecewise discontinuous functions. Attractive features of the AVS-FE method are its unconditional numerical stability

property (regardless of the underlying differential operator), its highly accurate flux approximations, and the ability to compute optimal test functions element-by-element.

In the following, we limit our focus to stationary scalar-valued convection-diffusion problems. In Section 2, we introduce the model problem of 2D scalar-valued convection-dominated diffusion, used notations, as well as a review of the AVS-FE methodology. Goal-oriented *a posteriori* error estimates are introduced in Sections 3 and 4. In Section 3, we introduce the goal-oriented error estimates for the AVS-FE method following the classical approach of Becker and Rannacher [7], i.e., the dual solution is sought in the (broken) test space, and present a numerical verification for the Laplace BVP. In Section 4, we present a new alternative approach to goal-oriented error estimation in which we seek C^0 or Raviart-Thomas AVS-FE approximations of the dual solution by using the underlying dual BVP. Numerical verifications investigating the effectivity and robustness of the new estimator are also presented in Section 4. Goal-oriented adaptive mesh refinements and numerical verifications are presented in Section 5. Lastly, conclusions and future work are discussed in Section 6.

2. Variationally Stable Analysis for Finite Element Computations

In this section, we introduce our convection-diffusion model problem and briefly present a review of the AVS-FE method. A more detailed introduction can be found in [1, 34].

2.1. Model Problem and Notation

Let $\Omega \subset \mathbb{R}^2$ be an open bounded domain with Lipschitz boundary $\partial\Omega$ and outward unit normal vector \mathbf{n} . The boundary $\partial\Omega$ consists of open subsections $\Gamma_D, \Gamma_N \subset \partial\Omega$, such that $\Gamma_D \cap \Gamma_N = \emptyset$ and $\partial\Omega = \overline{\Gamma_D \cup \Gamma_N}$. For our model problem, we consider the following linear convection-diffusion PDE in Ω with homogeneous Dirichlet condi-

tions on Γ_D and (possibly) non-homogeneous Neumann conditions on Γ_N :

Find u such that:

$$\begin{aligned} -\nabla \cdot (\mathbf{D}\nabla u) + \mathbf{b} \cdot \nabla u &= f, & \text{in } \Omega, \\ u &= 0, & \text{on } \Gamma_D, \\ \mathbf{D}\nabla u \cdot \mathbf{n} &= g, & \text{on } \Gamma_N, \end{aligned} \tag{1}$$

where \mathbf{D} denotes the second order diffusion tensor, with symmetric and elliptic coefficients $D_{ij} \in L^\infty(\Omega)$; $\mathbf{b} \in [L^\infty(\Omega)]^2$ the convection coefficient; $f \in L^2(\Omega)$ the source function; and $g \in H^{-1/2}(\Gamma_N)$ the Neumann data.

2.2. The AVS-FE Weak Formulation

For the sake of brevity, we only mention the few key points here of the derivation of a weak formulation for the AVS-FE method. We refer to [1, 34] for a more detailed treatment. We start by introducing a regular partition \mathcal{P}_h of Ω into elements K_m , such that:

$$\Omega = \text{int}\left(\bigcup_{K_m \in \mathcal{P}_h} \overline{K_m}\right), \quad K_m \cap K_n, \quad m \neq n.$$

The partition \mathcal{P}_h is such that any discontinuities in D_{ij} or \mathbf{b} are restricted to the boundaries of each element ∂K_m . We introduce an auxiliary flux variable $\mathbf{q} = \{q_x, q_y\}^T = \mathbf{D}\nabla u$, and recast (1) as a system of first-order PDEs:

Find $(u, \mathbf{q}) \in H^1(\Omega) \times H(\text{div}, \Omega)$ such that:

$$\begin{aligned} \mathbf{D}\nabla u - \mathbf{q} &= 0, & \text{in } \Omega, \\ -\nabla \cdot \mathbf{q} + \mathbf{b} \cdot \nabla u &= f, & \text{in } \Omega, \\ u &= 0, & \text{on } \Gamma_D, \\ \mathbf{q} \cdot \mathbf{n} &= g, & \text{on } \Gamma_N. \end{aligned} \tag{2}$$

By weakly enforcing the system of PDEs (2) *locally* on each element $K_m \in \mathcal{P}_h$, applying Green's identity to the term including the divergence of \mathbf{q} , applying Dirichlet and Neumann conditions on $\partial K_m \cap \Gamma_D$ and $\partial K_m \cap \Gamma_N$, respectively, and subsequently summing all the local contributions we arrive at the following equivalent global variational

formulation:

$$\boxed{\begin{aligned} &\text{Find } (u, \mathbf{q}) \in U(\Omega) \text{ such that:} \\ &B((u, \mathbf{q}); (v, \mathbf{w})) = F(v), \quad \forall (v, \mathbf{w}) \in V(\mathcal{P}_h). \end{aligned}} \quad (3)$$

Here, the bilinear form, $B : U(\Omega) \times V(\mathcal{P}_h) \rightarrow \mathbb{R}$, and linear functional, $F : V(\mathcal{P}_h) \rightarrow \mathbb{R}$, are defined as follows:

$$\begin{aligned} B((u, \mathbf{q}); (v, \mathbf{w})) &\stackrel{\text{def}}{=} \sum_{K_m \in \mathcal{P}_h} \left\{ \int_{K_m} \left[(\mathbf{D}\nabla u - \mathbf{q}) \cdot \mathbf{w}_m + \mathbf{q} \cdot \nabla v_m + (\mathbf{b} \cdot \nabla u) v_m \right] \mathrm{d}\mathbf{x} \right. \\ &\quad \left. - \oint_{\partial K_m \setminus \overline{\Gamma_D \cup \Gamma_N}} \gamma_n^m(\mathbf{q}) \gamma_0^m(v_m) \mathrm{d}s \right\}, \quad (4) \\ F(v) &\stackrel{\text{def}}{=} \sum_{K_m \in \mathcal{P}_h} \left\{ \int_{K_m} f v_m \mathrm{d}\mathbf{x} + \oint_{\partial K_m \cap \Gamma_N} g \gamma_0^m(v_m) \mathrm{d}s \right\}, \end{aligned}$$

where the trial and test function spaces, $U(\Omega)$ and $V(\mathcal{P}_h)$, are:

$$\begin{aligned} U(\Omega) &\stackrel{\text{def}}{=} \left\{ (u, \mathbf{q}) \in H^1(\Omega) \times H(\text{div}, \Omega) : \gamma_0^m(u)|_{\Gamma_D} = 0 \right\}, \\ V(\mathcal{P}_h) &\stackrel{\text{def}}{=} \left\{ (v, \mathbf{w}) \in H^1(\mathcal{P}_h) \times [L^2(\Omega)]^2 : \gamma_0^m(v_m)|_{\partial K_m \cap \Gamma_D} = 0, \forall K_m \in \mathcal{P}_h \right\}, \end{aligned} \quad (5)$$

in which the broken H^1 space is defined as:

$$H^1(\mathcal{P}_h) \stackrel{\text{def}}{=} \left\{ v \in L^2(\Omega) : v|_{K_m} \in H^1(K_m), \forall K_m \in \mathcal{P}_h \right\}, \quad (6)$$

and norms $\|\cdot\|_{U(\Omega)} : U(\Omega) \rightarrow [0, \infty)$ and $\|\cdot\|_{V(\mathcal{P}_h)} : V(\mathcal{P}_h) \rightarrow [0, \infty)$:

$$\begin{aligned} \|(u, \mathbf{q})\|_{U(\Omega)} &\stackrel{\text{def}}{=} \sqrt{\int_{\Omega} \left[\nabla u \cdot \nabla u + u^2 + (\nabla \cdot \mathbf{q})^2 + \mathbf{q} \cdot \mathbf{q} \right] \mathrm{d}\mathbf{x}}, \\ \|(v, \mathbf{w})\|_{V(\mathcal{P}_h)} &\stackrel{\text{def}}{=} \sqrt{\sum_{K_m \in \mathcal{P}_h} \int_{K_m} \left[h_m^2 \nabla v_m \cdot \nabla v_m + v_m^2 + \mathbf{w}_m \cdot \mathbf{w}_m \right] \mathrm{d}\mathbf{x}}, \end{aligned} \quad (7)$$

where $h_m = \text{diam}(K_m)$. The operators $\gamma_0^m : H^1(K_m) \rightarrow H^{1/2}(\partial K_m)$ and $\gamma_n^m : H(\text{div}, K_m) \rightarrow H^{-1/2}(\partial K_m)$ denote the local trace and normal trace operators (e.g., see [35]). Note that we employ an engineering notation convention here by using an integral representation of the boundary integrals rather than that of a duality pairing. The variational formulation (3) is essentially a DPG formulation in which only the space $V(\mathcal{P}_h)$ is broken.

Lemma 2.1 *Let $f \in (H^1(\mathcal{P}_h))'$ and $g \in H^{-1/2}(\Gamma_N)$. Then, the weak formulation (3) is well posed and has a unique solution.*

Proof: We provide only an outline of this proof as similar proofs are available in literature. We first note that the kernel of the underlying convection-diffusion differential operator is trivial and introduce an equivalent norm on $U(\Omega)$, the energy norm:

$$\|(u, \mathbf{q})\|_B \stackrel{\text{def}}{=} \sup_{(v, \mathbf{w}) \in V(\mathcal{P}_h) \setminus \{(0, \mathbf{0})\}} \frac{|B((u, \mathbf{q}); (v, \mathbf{w}))|}{\|(v, \mathbf{w})\|_{V(\mathcal{P}_h)}}. \quad (8)$$

In the philosophy of the DPG method, we identify an optimal test space, spanned by functions that are solutions of a Riesz representation problem:

$$((\hat{p}, \hat{\mathbf{r}}); (v, \mathbf{w}))_{V(\mathcal{P}_h)} = B((u, \mathbf{q}); (v, \mathbf{w})), \quad \forall (v, \mathbf{w}) \in V(\mathcal{P}_h). \quad (9)$$

Then, $B(\cdot, \cdot)$ satisfies the conditions of the Babuška Lax-Milgram Theorem [36] in terms of the energy norm (8) as the action of the bilinear form is equivalent to an inner product (9). We refer to the important results of [37], in the analysis of broken Hilbert spaces and variational formulations. In particular, it is shown that broken variational formulations based on differential operators with trivial kernels inherit the stability of their unbroken counterparts. □

Remark 2.1 *It is possible to derive other variational statements in which the trial space is continuous and the test space is discontinuous. These will be considered in a forthcoming paper.*

2.3. AVS-FE Discretization

The AVS-FE method seeks numerical approximations (u^h, \mathbf{q}^h) of (u, \mathbf{q}) of the variational formulation (3) by using classical FE bases for the trial functions (u^h, \mathbf{q}^h) , i.e., we represent the approximations as linear combinations of the trial basis functions $(e^i(\mathbf{x}), (E_x^j(\mathbf{x}), E_y^k(\mathbf{x}))) \in U^h(\Omega)$ and their corresponding degrees of freedom:

$$u^h(\mathbf{x}) = \sum_{i=1}^N u_i^h e^i(\mathbf{x}), \quad q_x^h(\mathbf{x}) = \sum_{j=1}^N q_x^{h,j} E_x^j(\mathbf{x}), \quad q_y^h(\mathbf{x}) = \sum_{k=1}^N q_y^{h,k} E_y^k(\mathbf{x}). \quad (10)$$

Since the solution space $U(\Omega)$ concerns $H^1(\Omega)$ and $H(\text{div}, \Omega)$ spaces, the FE discretizations can employ classical $C^0(\Omega)$ or Raviart-Thomas functions.

The test space $V(\mathcal{P}_h)$, however, is discontinuous, allowing us to construct piecewise discontinuous *optimal* test functions that yield unconditionally stable discretizations. These functions are constructed by employing the DPG philosophy [2–6] in which optimal test functions are defined by *global* weak problems. Thus, for the trial functions $e^i(\mathbf{x})$, $E_x^j(\mathbf{x})$, and $E_y^k(\mathbf{x})$, the corresponding global optimal test functions $(\tilde{e}^i, \tilde{\mathbf{E}}^i)$, $(\tilde{e}_x^j, \tilde{\mathbf{E}}_{\mathbf{x}}^j)$, and $(\tilde{e}_y^k, \tilde{\mathbf{E}}_{\mathbf{y}}^k)$ are the solutions of the following Riesz representation problems [1, 34], respectively:

$$\begin{aligned} \left((r, \mathbf{z}); (\tilde{e}^i, \tilde{\mathbf{E}}^i) \right)_{V(\mathcal{P}_h)} &= B((e^i, \mathbf{0}); (r, \mathbf{z})), \quad \forall (r, \mathbf{z}) \in V(\mathcal{P}_h), \quad i = 1, \dots, N, \\ \left((r, \mathbf{z}); (\tilde{e}_x^j, \tilde{\mathbf{E}}_{\mathbf{x}}^j) \right)_{V(\mathcal{P}_h)} &= B((0, (E_x^j, \mathbf{0})); (r, \mathbf{z})), \quad \forall (r, \mathbf{z}) \in V(\mathcal{P}_h), \quad j = 1, \dots, N, \\ \left((r, \mathbf{z}); (\tilde{e}_y^k, \tilde{\mathbf{E}}_{\mathbf{y}}^k) \right)_{V(\mathcal{P}_h)} &= B((0, (0, E_y^k)); (r, \mathbf{z})), \quad \forall (r, \mathbf{z}) \in V(\mathcal{P}_h), \quad k = 1, \dots, N, \end{aligned} \quad (11)$$

where $((\cdot, \cdot); (\cdot, \cdot))_{V(\mathcal{P}_h)}$ denotes the broken inner product on $V(\mathcal{P}_h)$, defined by:

$$((r, \mathbf{z}); (v, \mathbf{w}))_{V(\mathcal{P}_h)} \stackrel{\text{def}}{=} \sum_{K_m \in \mathcal{P}_h} \int_{K_m} \left[h_m^2 \nabla r_m \cdot \nabla v_m + r_m v_m + \mathbf{z}_m \cdot \mathbf{w}_m \right] \text{d}\mathbf{x}. \quad (12)$$

Remark 2.2 Remarkably, the broken nature of the test space $V(\mathcal{P}_h)$ allows us to compute numerical approximations of the local restrictions of the optimal test functions in a completely decoupled fashion (see [1, 34] for details). Thus, we solve local restrictions of (11), e.g.,

$$\begin{aligned} \left((r, \mathbf{z}); (\tilde{e}_h^i, \tilde{\mathbf{E}}_h^i) \right)_{V(K_m)} &= B_{|K_m}((e^i, \mathbf{0}); (r, \mathbf{z})), \quad \forall (r, \mathbf{z}) \in V(K_m), \\ \left((r, \mathbf{z}); (\tilde{e}_{x_h}^j, \tilde{\mathbf{E}}_{x_h}^j) \right)_{V(K_m)} &= B_{|K_m}((0, (E_x^j, \mathbf{0})); (r, \mathbf{z})), \quad \forall (r, \mathbf{z}) \in V(K_m), \\ \left((r, \mathbf{z}); (\tilde{e}_{y_h}^k, \tilde{\mathbf{E}}_{y_h}^k) \right)_{V(K_m)} &= B_{|K_m}((0, (0, E_y^k)); (r, \mathbf{z})), \quad \forall (r, \mathbf{z}) \in V(K_m), \end{aligned} \quad (13)$$

where $B_{|K_m}(\cdot; \cdot)$ denotes the restriction of $B(\cdot; \cdot)$ to the element K_m . Hence, while the optimal test functions are defined by global weak statements, their numerical computation can be performed element-by-element (see, e.g., [38] for a detailed discussion on this element-wise assembly process).

Remark 2.3 Numerical verifications reveal that the local test functions can be computed by using a degree of approximation that is identical to the degree of approximation of their corresponding trial functions.

Remark 2.4 The choice of C^0 or Raviart-Thomas trial functions has the consequence that the optimal test functions have the same support as the trial functions [1, 34].

Finally, we introduce the FE discretization of (3) governing the AVS-FE approximation $(u^h, \mathbf{q}^h) \in U(\Omega)$ of (u, \mathbf{q}) :

$$\boxed{\begin{aligned} \text{Find } (u^h, \mathbf{q}^h) \in U^h(\Omega) \text{ such that:} \\ B((u^h, \mathbf{q}^h); (v^*, \mathbf{w}^*)) = F(v^*), \quad \forall (v^*, \mathbf{w}^*) \in V^*(\mathcal{P}_h), \end{aligned}} \quad (14)$$

where the finite dimensional subspace of test functions $V^*(\mathcal{P}_h) \subset V(\mathcal{P}_h)$ is spanned by the numerical approximations of the test functions $\{(\tilde{e}_h^i, \tilde{\mathbf{E}}_h^i)\}_{i=1}^N$, $\{(\tilde{e}_{x_h}^j, \tilde{\mathbf{E}}_{x_h}^j)\}_{j=1}^N$, and $\{(\tilde{e}_{y_h}^k, \tilde{\mathbf{E}}_{y_h}^k)\}_{k=1}^N$, as computed from the test function problems (11) and (13).

Since we use the DPG methodology here to construct the optimal test space $V^*(\mathcal{P}_h)$, the discrete problem (14) satisfies the conditions of the Babuška Lax-Milgram Theorem with continuity and inf-sup constants of the continuous problem (3) scaled by the continuity constant of a Fortin type operator [39]. It is therefore unconditionally stable for any choice of mesh parameters h_m and p_m . The corresponding global stiffness matrices are symmetric and positive definite.

In the following sections we derive error estimates in terms of user defined QoIs of the solution. The QoIs are represented in terms of continuous linear functionals $Q_i : U(\Omega) \rightarrow \mathbb{R}, i = 1, 2, \dots, N_Q$, for example:

$$Q_i(u, \mathbf{q}) = \frac{1}{|\omega|} \int_{\omega} u \, \mathbf{dx}, \quad (15)$$

Thus, the goal is to estimate the error $Q(u - u^h, \mathbf{q} - \mathbf{q}^h)$. We introduce residual based *a posteriori* estimates by taking two distinctive approaches to the solution of the dual problem. The first follows the approach introduced by Becker and Rannacher [7] and therefore seeks a dual solution in the broken primal test space $V(\mathcal{P}_h)$. The second approach concerns an alternative approach in which the AVS-FE solution of the under-

lying strong form of the dual problem is sought in a $H^1(\Omega) \times H(\text{div}, \Omega)$ subspace of the primal test space.

3. Goal-Oriented Error Estimation - Classical Approach

Following Becker and Rannacher [7, 10, 13] we state the following classical lemma of goal-oriented error estimation:

Lemma 3.1 *Let (u, \mathbf{q}) be the exact solution of the first-order system (2), (u^h, \mathbf{q}^h) the AVS-FE approximation of (u, \mathbf{q}) per (14), and $(p_i, \mathbf{r}_i) \in V(\mathcal{P}_h)$ a dual solution for each QoI, governed by:*

$$\boxed{\begin{array}{l} \text{Find } (p_i, \mathbf{r}_i) \in V(\mathcal{P}_h) \text{ such that:} \\ B((v, \mathbf{w}); (p_i, \mathbf{r}_i)) = Q_i(v, \mathbf{w}), \quad \forall (v, \mathbf{w}) \in U(\Omega). \end{array}} \quad (16)$$

Then, the error in the QoI $\mathcal{E}_i(u^h, \mathbf{q}^h) = Q_i(u - u^h, \mathbf{q} - \mathbf{q}^h)$, is governed by the identity:

$$\boxed{\mathcal{E}_i(u^h, \mathbf{q}^h) \stackrel{\text{def}}{=} \mathcal{R}_h((u^h, \mathbf{q}^h); (p_i, \mathbf{r}_i)),} \quad (17)$$

where $\mathcal{R}_h((\cdot, \cdot); (\cdot, \cdot))$ is the residual functional:

$$\mathcal{R}_h((u, \mathbf{q}); (v, \mathbf{w})) = F(v) - B((u, \mathbf{q}); (v, \mathbf{w})). \quad (18)$$

Remark 3.1 *Analogous to the well-posedness of the primal problem (3) (see Lemma 2.1), the dual problems (16) are well posed (since the kernel of the adjoint operator of $B(\cdot, \cdot)$ is also trivial).*

To compute estimates of the error $\mathcal{E}_i(u^h, \mathbf{q}^h)$ through (17), we compute approximations of the dual solutions (p_i^h, \mathbf{r}_i^h) by following the classical approach of [7, 10, 40]. Thus, for a given QoI, the approximate dual solution (p^h, \mathbf{r}^h) is governed by:

$$\boxed{\begin{array}{l} \text{Find } (p^h, \mathbf{r}^h) \in V^*(\mathcal{P}_h) \text{ such that:} \\ B((v^h, \mathbf{w}^h); (p^h, \mathbf{r}^h)) = Q(v^h, \mathbf{w}^h), \quad \forall (v^h, \mathbf{w}^h) \in U^h(\Omega). \end{array}} \quad (19)$$

We seek (p^h, \mathbf{r}^h) in the discrete, broken space $V^*(\mathcal{P}_h)$ spanned by $(\tilde{e}_h^i, \tilde{\mathbf{E}}_h^i)$ of the local Riesz representation problems (13). Hence, we use the same element partition \mathcal{P}_h of Ω

as we used for the primal problem to compute (p^h, \mathbf{r}^h) . However, due to the Galerkin orthogonality condition of the numerical approximation error, the approximate dual solution has to be sought by using polynomial approximations that are of higher order than the trial functions used to solve the discrete primal problem (14). We choose $p + 1$. Hence, the unconditional numerical stability of the AVS-FE methodology will allow the computation of approximate dual solutions (p_i^h, \mathbf{r}_i^h) for any choice of mesh parameters h_m and p_m . The estimated error η_{est} in the quantity of interest is then computed by:

$$\eta_{est} \approx \mathcal{E}_i^h(u^h, \mathbf{q}^h) = \mathcal{R}_h((u^h, \mathbf{q}^h); (p_i^h, \mathbf{r}_i^h)) \quad (20)$$

This classical approach has been shown to be very successful in a wide range of applications, especially those in which the differential operator is self-adjoint (e.g., see [10, 40]).

As a numerical verification of this estimator, we consider the Laplace problem on the unit square $\Omega = (0, 1) \times (0, 1) \subset \mathbb{R}^2$ with homogeneous Dirichlet boundary conditions:

$$\begin{aligned} -\Delta u &= f, & \text{in } \Omega, \\ u &= 0, & \text{on } \partial\Omega. \end{aligned} \quad (21)$$

The source function f , is chosen such that the exact solution is given by:

$$u(x, y) = e^{[50(x^2-x)(y^2-y)]} - 1.$$

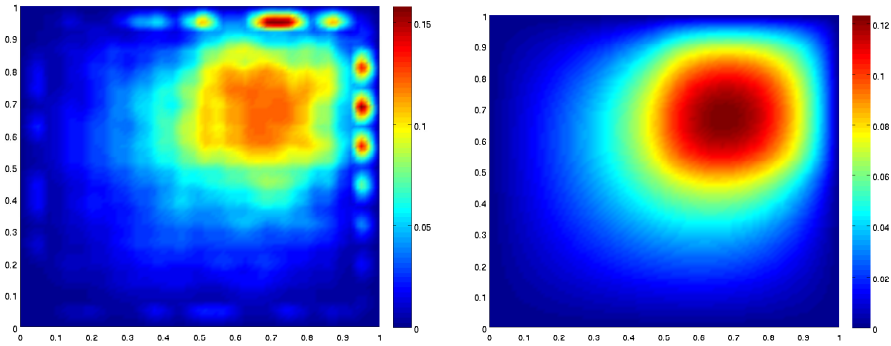
The QoI is chosen to be the average of the solution u in the region $\omega = (0.5, 1) \times (0.5, 1) \subset \Omega$:

$$\mathcal{Q}(u, \mathbf{q}) = \frac{1}{|\omega|} \int_{\omega} u \, d\mathbf{x}. \quad (22)$$

To estimate the error in this QoI (22) we apply the AVS-FE discretization to the primal and dual problem with polynomial degrees of approximation of 2 and 3, respectively. As in [1], we use C^0 continuous bases for both trial variables u^h and \mathbf{q}^h of the same polynomial degree, while for p^h and \mathbf{r}^h we use the optimal bases determined by the Riesz representation problems (11). The mesh initial mesh partition used consists of a single quadrilateral element. Subsequent meshes are a sequence uniformly refined from the initial single element. To assess the quality of the error estimate, we introduce

Table 1: Error estimation results for the Laplace problem with QoI (22) using the classical approach, i.e., through (19) and (20).

Primal dofs	$Q(u, \mathbf{q}) - Q(u^h, \mathbf{q}^h)$	Dual dofs	η_{est}	\mathcal{I}_{eff}
27	-9.2601e+00	48	-1.0601e+01	1.145
75	2.3191e-02	147	-7.5337e-02	-0.325
243	1.8610e-02	507	3.4581e-02	1.858
867	-3.7844e-05	1875	-3.8616e-04	10.204
3267	-2.5778e-05	7203	-5.3075e-05	2.059



(a) Dual solution in the classical approach.

(b) Overkill solution.

Figure 1: Dual solution p^h .

the effectivity index:

$$\mathcal{I}_{eff} = \frac{\eta_{est}}{Q(u, \mathbf{q}) - Q(u^h, \mathbf{q}^h)}. \quad (23)$$

In Table 1, we present the error estimates for increasingly refined meshes. It appears that the magnitude of the estimated error decreases monotonically. However, the results for the effectivity index \mathcal{I}_{eff} reveal that the estimates generally have poor accuracy nor exhibit any consistent evolution during the uniform h -refinements. We suspect that since the continuity of the dual solution is enforced weakly in (16), it prohibits from adequately resolving the discretization of the dual solution on the used meshes. We suspect that without drastically changing the formulation using jump and/or average operators on the mesh skeleton as one would in, e.g, discontinuous Galerkin methods

the discontinuous solutions will not provide adequate resolution of the dual solution. Comparison of the approximate solution p^h in Figure 1 to an overkill approximation of p in Figure 1(b), reveals internal oscillations in p^h in each element as well as along the global boundaries. The overkill solution is obtained using a Galerkin FE method for the underlying known dual BVP on a highly refined uniform mesh of quadratic quadrilateral elements. While bounded, these contribute to the poor quality of the error estimates. These observed oscillations show no consistent behavior during mesh refinements. This behavior persists for numerical verifications in which the degree of approximation for the dual problem is $p_{dual} = p_{primal} + 2, p_{primal} + 3$ etc. Another factor that plays a role here can be deduced from DPG* techniques [41] since the dual problem (19) can be interpreted as a modified DPG* form. In particular, it is shown in [41] that the regularity of the domain Ω is a crucial factor in the accuracy of the dual solution.

4. Goal-Oriented Error Estimation - Alternative Approach

Since we suspect that the poor accuracy of the estimator via the classical approach is likely caused by the discontinuous character of the numerical approximation of the dual solutions (p^h, \mathbf{r}^h) , we propose an alternative approach for computing (p^h, \mathbf{r}^h) . Instead of seeking discontinuous discrete approximations of the dual solution by using the corresponding dual weak formulation (16) of the primal problem (3), we rather reconsider the underlying strong form of each dual problem, i.e.,

Find $(p_i, \mathbf{r}_i) \in H^1(\Omega) \times H(\text{div}, \Omega)$ such that:

$$\begin{aligned} -\mathbf{r}_i + \nabla p_i &= \mathbf{0}, & \text{in } \Omega, \\ -\nabla \cdot (\mathbf{D}\mathbf{r}_i) - \mathbf{b} \cdot \nabla p_i &= \theta_i, & \text{in } \Omega, \\ p_i &= 0, & \text{on } \partial\Omega, \end{aligned} \tag{24}$$

where $\theta_i \in U'(\Omega)$ is such that $\langle \theta_i, (u, \mathbf{q}) \rangle_{U' \times U} = Q_i(u, \mathbf{q})$. Comparison of (24) and the first order system for the primal problem (2) shows that the diffusion tensor has shifted and the signs in the vector valued PDE has changed. The reason is that (24) is the natural form of the distributional first order dual BVP when derived from the AVS-FE

weak formulation. We subsequently derive a weak statement governing (p_i, \mathbf{r}_i) by using the same approach as the applied to the derivation of the weak statement of the primal problem (see Section 2). Thus, we seek $p_i \in H^1(\Omega)$, $\mathbf{r}_i \in H(\text{div}, \Omega)$ and employ test spaces for the dual problem that are broken. Hence, p_i and \mathbf{r}_i belong to the same globally (weakly) continuous function spaces as the primal solution (u, \mathbf{q}) . To derive the dual weak statement, we follow the derivation in [1] and enforce the system (24) weakly on each element $K_m \in \mathcal{P}_h$, apply Green's Identity, enforce boundary conditions, and arrive at the following weak statement:

$$\boxed{\begin{aligned} \text{Find } (p_i, \mathbf{r}_i) \in U(\Omega) \text{ such that:} \\ \hat{B}((v, \mathbf{w}); (p_i, \mathbf{r}_i)) = Q_i(v, \mathbf{w}), \quad \forall (v, \mathbf{w}) \in W(\mathcal{P}_h), \end{aligned}} \quad (25)$$

where:

$$\begin{aligned} \hat{B}((v, \mathbf{w}); (p_i, \mathbf{r}_i)) = \sum_{K_m \in \mathcal{P}_h} \left\{ \int_{K_m} \left[(\nabla p_i - \mathbf{r}_i) \cdot \mathbf{w}_m + \mathbf{D} \mathbf{r}_i \cdot \nabla v_m - (\mathbf{b} \cdot \nabla p_i) v_m \right] dx \right. \\ \left. - \oint_{\partial K_m \setminus \partial \Omega} \gamma_{\mathbf{n}}^m(\mathbf{D} \mathbf{r}_i) \gamma_0^m(v_m) ds \right\}, \end{aligned} \quad (26)$$

and:

$$W(\mathcal{P}_h) \stackrel{\text{def}}{=} \left\{ (v, \mathbf{w}) \in H^1(\mathcal{P}_h) \times [L^2(\Omega)]^2 : \gamma_0^m(v_m)|_{\partial K_m \cap \partial \Omega} = 0, \forall K_m \in \mathcal{P}_h \right\}. \quad (27)$$

It should be noted here that $\hat{B}(\cdot; \cdot)$ and $B(\cdot; \cdot)$ differ in the sign in front of the convection vector \mathbf{b} due to the non-self adjoint character of the differential operator of (1). Now, to ensure the unconditional stability of the discrete dual problem we use optimal discontinuous test functions $(\tilde{e}^i, \tilde{\mathbf{E}}^i)$, $(\tilde{e}_x^j, \tilde{\mathbf{E}}_x^j)$, and $(\tilde{e}_y^k, \tilde{\mathbf{E}}_y^k)$ for the dual problem that are solutions of the following (Riesz) weak problems:

$$\begin{aligned} \left((x, \mathbf{z}); (\tilde{e}^i, \tilde{\mathbf{E}}^i) \right)_{V(\mathcal{P}_h)} &= \hat{B}((x, \mathbf{z}); (e^i, \mathbf{0})), \quad \forall (x, \mathbf{z}) \in V(\mathcal{P}_h), \quad i = 1, \dots, N, \\ \left((x, \mathbf{z}); (\tilde{e}_x^j, \tilde{\mathbf{E}}_x^j) \right)_{V(\mathcal{P}_h)} &= \hat{B}((x, \mathbf{z}); (0, (E_x^j, \mathbf{0}))), \quad \forall (x, \mathbf{z}) \in V(\mathcal{P}_h), \quad j = 1, \dots, N, \\ \left((x, \mathbf{z}); (\tilde{e}_y^k, \tilde{\mathbf{E}}_y^k) \right)_{V(\mathcal{P}_h)} &= \hat{B}((x, \mathbf{z}); (0, (0, E_y^k))), \quad \forall (x, \mathbf{z}) \in V(\mathcal{P}_h), \quad k = 1, \dots, N. \end{aligned} \quad (28)$$

Remark 4.1 *The vector valued dual solution \mathbf{Dr}_i belongs to $H(\text{div}, \Omega)$ due to the boundary integral $\oint_{\partial K_m \setminus \partial \Omega} \boldsymbol{\gamma}_n^m(\mathbf{Dr}_i) \boldsymbol{\gamma}_0^m(v_m) \, ds$ in (25). For this integral to be Lebesgue integrable, \mathbf{Dr}_i has to belong to $H^{-1/2}(\partial K_m)$ which implies $\mathbf{Dr}_i \in H(\text{div}, \Omega)$.*

We then establish the error estimator $\hat{\eta}_{est}$ by using the new dual solutions:

$$\hat{\eta}_{est} \approx \mathcal{E}_i^{ch}(u^h, \mathbf{q}^h) = \mathcal{R}_h((u^h, \mathbf{q}^h); (p_i^h, \mathbf{r}_i^h)) \quad (29)$$

Having established the new alternative error estimates, we propose to employ an error indicator ε_m corresponding to the restriction of the goal-oriented error estimate $\hat{\eta}_{est}$ in mesh adaptive refinements, i.e.,

$$\varepsilon_m = \mathcal{R}_h|_{K_m}((u^h, \mathbf{q}^h); (p_i^h, \mathbf{r}_i^h)). \quad (30)$$

Remark 4.2 *We note that the philosophy we advocate here for the dual problem was also proposed for the consideration of adjoint equations in inverse FE methods by considering the strong form of the adjoint equation by Bramwell in [42].*

4.1. Numerical Verification - Diffusion Problem

We again solve (21) using identical meshes and degrees of approximation as in Section 3, i.e., quadratic primal and cubic dual approximations, respectively. In this alternative approach, we seek C^0 continuous solutions to both the primal and dual problems in which the scalar and flux variables are of the same polynomial degree. Again, we assess the quality of the error estimate with the effectivity index:

$$\hat{\mathcal{J}}_{eff} = \frac{\hat{\eta}_{est}}{Q(u, \mathbf{q}) - Q(u^h, \mathbf{q}^h)}. \quad (31)$$

In Table 2, we show the results for the error estimates for uniform mesh refinements. As in Section 3, the magnitude of the error decreases monotonically. However, the effectivity index now shows that the estimates have very good accuracy with values close to unity. Furthermore, comparison of Figure 2 of the dual AVS-FE solution to an overkill solution reveals that there are no oscillations at element interiors and global boundaries.

Table 2: Error estimation results for the Laplace problem with QoI (22) using the new alternative approach, i.e., through (25) and (20).

Primal dofs	$Q(u, \mathbf{q}) - Q(u^h, \mathbf{q}^h)$	Dual dofs	$\hat{\eta}_{est}$	$\hat{\mathcal{I}}_{eff}$
27	-9.2601e+00	48	-1.0601e+01	1.145
75	2.3192e-02	147	3.4410e-02	1.484
243	1.8610e-02	507	1.8602e-02	0.999
867	-3.7845e-05	1875	-3.6160e-05	0.956
3267	-2.5778e-05	7203	-2.3479e-05	0.911

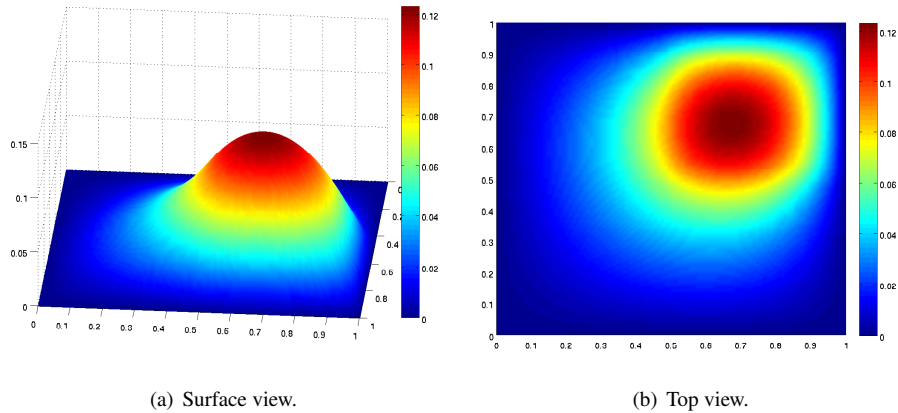


Figure 2: C^0 dual solution p^h obtained by the new alternative approach through (25) on a uniform mesh with 3267 dofs.

4.2. Numerical Verifications - Convection-Dominated Diffusion

Next, we consider a more challenging case of a convection-dominated diffusion problem. In this subsection, we consider a simplified form of our model problem (1) on the unit square with homogeneous Dirichlet boundary conditions:

$$\begin{aligned}
 -\frac{1}{\text{Pe}}\Delta u + \mathbf{b} \cdot \nabla u &= f, & \text{in } \Omega = (0, 1) \times (0, 1), \\
 u &= 0, & \text{on } \partial\Omega,
 \end{aligned} \tag{32}$$

where the Péclet number $\text{Pe} = 100$ is and $\mathbf{b} = \{1, 1\}^T$ the convection coefficient. We consider the case of (32) in which the above source function f is chosen such that the

exact solution is given by:

$$u(x, y) = \left[x + \frac{e^{\text{Pe} \cdot b_x \cdot x} - 1}{1 - e^{\text{Pe} \cdot b_x}} \right] \left[y + \frac{e^{\text{Pe} \cdot b_y \cdot y} - 1}{1 - e^{\text{Pe} \cdot b_y}} \right]. \quad (33)$$

Thus, the solution exhibits boundary layers along $x = 1$ and $y = 1$ with a width of $\frac{1}{\text{Pe}} = 0.01$, as shown in Figure 3.

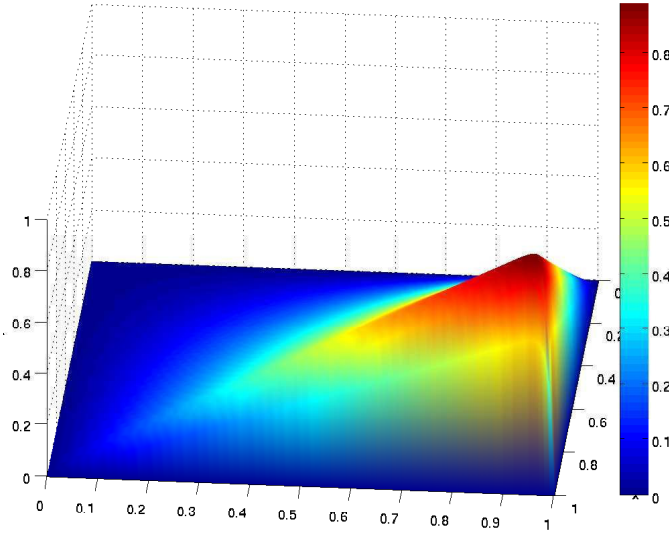


Figure 3: Exact solution u of the simplified model problem (32) with $\mathbf{b} = \{1, 1\}^T$ and $\text{Pe} = 100$.

4.2.1. Uniform Meshes

First, we consider uniform meshes consisting of quadrilateral elements. The first QoI is chosen as in (22), i.e., the average solution u in the top right quadrant of the unit square. In Figure 4, we show the corresponding overkill solution p of the dual problem. The dual solution, similar to the primal, exhibits boundary layers. However, as the direction of the convection is reversed from the primal problem, the layers are at opposite edges of the domain. To verify the new estimator $\hat{\eta}_{est}$ we employ AVS-FE discretizations of the primal and dual problem with polynomial degrees of approximation of 2 and 3, respectively. The corresponding numerical results are illustrated in Table 3. The effectivity indices show that the error estimator accurately measures the

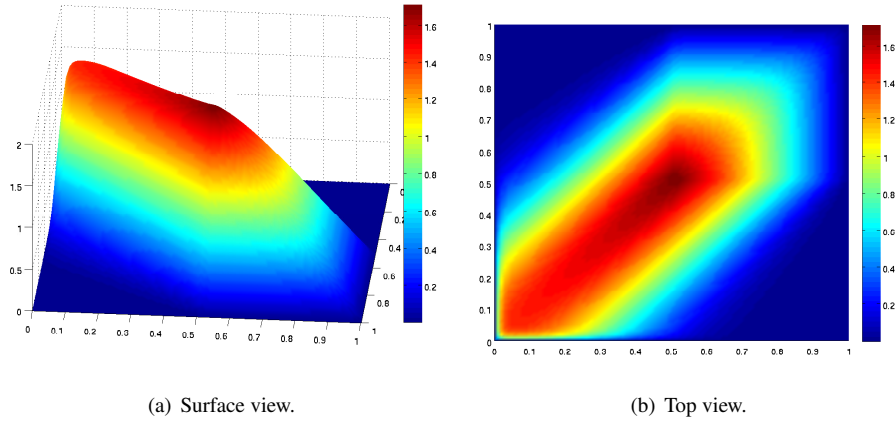


Figure 4: Overkill solution p of the dual problem with $\mathbf{b} = \{1, 1\}^T$ and $\text{Pe} = 100$.

approximation error. For initial, coarse, meshes the effectivity index may not be very

Table 3: Results for the convection-dominated diffusion problem (32) with QoI (22) for uniform mesh refinements and $\text{Pe} = 100$.

Primal dofs	$Q(u, \mathbf{q}) - Q(u^h, \mathbf{q}^h)$	Dual dofs	$\hat{\eta}_{est}$	\mathcal{I}_{eff}
243	2.8825e-01	507	1.6140e-01	0.599
867	1.7711e-01	1875	1.5010e-01	0.848
3267	6.7393e-02	7203	6.5077e-02	0.966
12675	1.3225e-02	28227	1.3158e-02	0.995
49923	1.3918e-03	111747	1.3909e-03	0.999
198147	1.0321e-04	444675	1.0321e-04	0.999

close to unity, but is of the same order of magnitude as the exact error. As the uniform meshes are further refined, the estimate converges to the exact error and delivers highly accurate predictions of the error with the effectivity index \mathcal{I}_{eff} very close to unity. The rate of convergence of the error estimate in Table 3 approaches the often observed superconvergence rate of 4 for bounded linear QoIs as reported by Giles and Süli in [11].

The second QoI we consider is the average flux in the x -direction in the same quad-

rant of the unit square as before, i.e., $\omega = (0.5, 1) \times (0.5, 1)$. First, we consider the the derivative of the base variable u :

$$Q(u, \mathbf{q}) = \frac{1}{|\omega|} \int_{\omega} \frac{\partial u}{\partial x} \, d\mathbf{x}, \quad (34)$$

and second, the flux variable:

$$Q(u, \mathbf{q}) = \frac{1}{|\omega|} \int_{\omega} q_x \, d\mathbf{x}. \quad (35)$$

The polynomial degrees of approximation are now 1 and 2 for the primal and dual problem, respectively. As shown in Tables 4 and 5, the errors in a QoI in terms of a

Table 4: Results for the convection-dominated diffusion problem (32), with QoI (34) for uniform mesh refinements and $Pe = 100$.

Primal dofs	$Q(u, \mathbf{q}) - Q(u^h, \mathbf{q}^h)$	Dual dofs	$\hat{\eta}_{est}$	\mathcal{J}_{eff}
867	-3.6294e-01	3267	1.9153e-01	-0.5277
3267	-1.826e-01	12675	-2.1098e-03	0.0157
12675	-6.8810e-02	49923	-4.3560e-02	0.6881
49923	-1.7803e-02	198147	-1.1682e-02	0.9448

Table 5: Results for the convection-dominated diffusion problem (32), with QoI (35) for uniform mesh refinements and $Pe = 100$.

Primal dofs	$Q(u, \mathbf{q}) - Q(u^h, \mathbf{q}^h)$	Dual dofs	$\hat{\eta}_{est}$	\mathcal{J}_{eff}
867	8.7745e-03	3267	1.1171e-02	1.3346
3267	2.7558e-03	12675	3.8641e-03	1.4021
12675	7.3292e-04	49923	8.4109e-04	1.1476
49923	1.8478e-04	198147	1.8759e-04	1.0152

derivative are slightly higher than those of the preceding numerical verification for the former case, which is to be expected (see [1, 34]). The results in the latter are superior, again this is to be expected since the approximation of derivatives is generally less accurate. While for coarse meshes the estimate in terms of the QoI with the derivative does not accurately assess the error, it does capture the right order of magnitude

and improves significantly upon mesh refinements as the effectivity indices \mathcal{I}_{eff} approaches unity. However, the estimate in terms of the flux variable exhibits significant accuracy even for coarse meshes.

The final numerical verification we consider for uniform mesh partitions is a QoI that is the average flux in the x -direction along the line segment on the left edge of the unit square, i.e., ω is the line segment from $y = 0.5$ to $y = 0.75$:

$$Q(u, \mathbf{q}) = \frac{1}{|\omega|} \int_{\omega} q_x \, dx. \quad (36)$$

This type of QoI is particularly important in engineering design applications where fluxes or stresses and strains are critical design parameters. Furthermore, for such quantities, classical methods often require enhancement techniques to achieve adequate accuracy such as the biharmonic smoothing introduced in [11]. Furthermore, to show that the error estimate remains highly accurate when the error in the QoI becomes very small we pick $Pe = 10$. The polynomial degrees of approximation are 2 and 3 for the primal and dual problem, respectively.

Table 6: Results for the convection-dominated diffusion problem (32), with QoI (36) for uniform mesh refinements and $Pe = 10$.

Primal dofs	$Q(u, \mathbf{q}) - Q(u^h, \mathbf{q}^h)$	Dual dofs	$\hat{\eta}_{est}$	\mathcal{I}_{eff}
867	-3.0174e-04	3267	-7.1583e-05	0.2372
3267	-2.0855e-05	12675	-1.6377e-05	0.7853
12675	-1.3401e-06	49923	-1.3090e-06	0.9768
49923	-8.4335e-08	198147	-8.5814e-08	1.0175

The results in Table 6 show that the alternative approach is capable of estimating the error in terms of local QoIs pertaining to fluxes across boundaries. As the meshes become finer, the estimate becomes more accurate. However, for the coarsest mesh, i.e., the first row in Table 6, the estimate is still within an order of magnitude of the exact error. As the error becomes very small, the new alternative method still provides accurate estimates without the need for additional enhancement techniques.

4.2.2. Non-Uniform Mesh

So far, we have only considered rectangular uniform meshes. To provide a more realistic scenario, as encountered in engineering applications, we consider a mesh in which the elements are skewed and the element edges do not align with the direction of the convection (see Figure 5). We consider the same convection-dominated diffusion

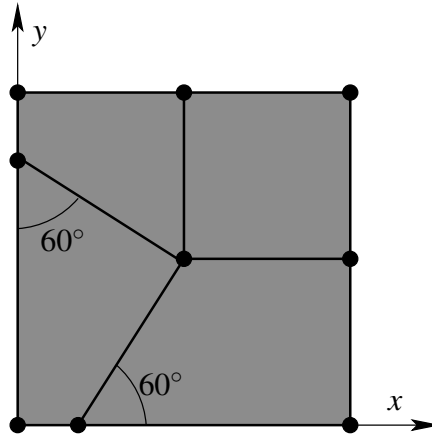


Figure 5: Poorly constructed skewed mesh.

PDE (32), but now with $Pe = 200$. The QoI is again the average of the solution u in the region $\omega = (0.5, 1) \times (0.5, 1)$ (i.e., see (22)).

In Table 7, we list the results for the case in which the primal degree of approximation is 2, and the dual degree of approximation is 3. After each computation of the primal and dual solutions, all elements in the mesh are uniformly refined. As in previous examples, the effectivity index is close to unity, indicating that the estimator can be successfully employed for skewed meshes.

4.2.3. Raviart-Thomas Approximation Of Fluxes

Until this point, we have used C^0 approximations for both trial variables, as our experience has shown this to yield good approximations [1]. Because $\mathbf{q} \in H(\text{div}, \Omega)$, the C^0 approximations have an overly restrictive regularity. Commonly, in mixed FE methods, Raviart-Thomas rather than $C^0(\Omega)$ approximations are used. To show our approach also provides reliable estimates for such approximations we now consider the

Table 7: Results for the convection-dominated diffusion problem (32), with QoI (22) for uniform mesh refinements of a skewed initial mesh partition and $Pe = 200$.

Primal dofs	$Q(u, \mathbf{q}) - Q(u^h, \mathbf{q}^h)$	Dual dofs	$\hat{\eta}_{est}$	$\hat{\mathcal{I}}_{eff}$
867	1.9480e-01	1875	2.5397e-01	1.304
3267	3.9104e-02	7203	4.6311e-02	1.184
12675	4.0197e-03	28227	4.2989e-03	1.069
49923	1.7641e-04	111747	1.7937e-04	1.017
198147	5.0934e-06	444675	5.0988e-06	1.001

case in which we use a Raviart-Thomas approximation [35, 43, 44] for the variables in $H(\text{div}, \Omega)$ (i.e., \mathbf{q} and \mathbf{r}). We again consider the case where $\mathbf{b} = \{1, 1\}^T$, $Pe = 100$, and choose the same QoI (22), i.e., the average solution u in the top right quadrant of the unit square. To approximate the error in the QoI, we now use tetrahedral elements in which u^h, p^h are discretized with C^0 polynomials, while $\mathbf{q}^h, \mathbf{r}^h$ are discretized using Raviart-Thomas bases. The initial mesh consists of two triangles which are refined uniformly after each computation using orders of approximation of 2 for the primal and 3 for the dual problems, respectively.

For the same element partition, we achieve slightly higher accuracy at a slightly lower number of degrees of freedom for C^0 approximations versus Raviart-Thomas approximations for \mathbf{q}^h , as evident from Tables 8 and 9. Comparison of the results in these tables also reveal that there is no significant difference between the two approximations in terms of the accuracy of the error estimates. Raviart-Thomas approximations are used in mixed FE methods as they result in stable FE approximations, as well as consistency of the approximations. Contrarily, C^0 approximations for $H(\text{div}, \Omega)$ variables cannot be employed in the same straightforward manner for mixed FE methods and will lead to a violation of discrete *inf-sup* conditions [44]. However, in the AVS-FE method, this stability problem is avoided by employing the DPG philosophy and optimal test functions that ensure the discrete *inf-sup* condition.

Table 8: Results for the convection-dominated diffusion problem (32), with QoI (22) for uniform mesh refinements with a C^0 approximation for both variables and $Pe = 100$.

Primal dofs	$Q(u, \mathbf{q}) - Q(u^h, \mathbf{q}^h)$	$\ \mathbf{q} - \mathbf{q}^h\ _{L^2(\Omega)}$	Dual dofs	$\hat{\eta}_{est}$	\mathcal{J}_{eff}
243	3.1381e-01	8.3021e-02	507	1.7312e-01	0.552
867	1.9449e-01	5.7260e-02	1875	1.5716e-01	0.808
3267	7.3123e-02	3.3955e-02	7203	7.2499e-02	0.991
12675	1.3955e-02	1.4723e-02	28227	1.4085e-02	1.009
49923	1.4397e-03	4.6769e-03	111747	1.4432e-03	1.002

Table 9: Results for the convection-dominated diffusion problem (32), with QoI (22) for uniform mesh refinements with a Raviart-Thomas approximation of fluxes and $Pe = 100$.

Primal dofs	$Q(u, \mathbf{q}) - Q(u^h, \mathbf{q}^h)$	$\ \mathbf{q} - \mathbf{q}^h\ _{L^2(\Omega)}$	Dual dofs	$\hat{\eta}_{est}$	\mathcal{J}_{eff}
257	3.5772e-01	9.0700e-02	529	1.8006e-01	0.503
961	2.3563e-01	6.1567e-02	2017	1.7260e-01	0.733
3713	9.9548e-02	3.7049e-02	7873	9.5166e-02	0.956
14593	2.0993e-02	1.7127e-02	31105	2.1050e-02	1.003
57857	2.2705e-03	5.7263e-03	123649	2.2741e-03	1.001

5. Adaptive Mesh Refinement

To demonstrate application of the new alternative error estimate (20) and the resulting error indicators (30) in an h -adaptive process, we use the same form of our model problem, i.e., $\mathbf{b} = \{1, 1\}^T$ and $Pe = 100$. As the adaptive strategy for goal-oriented mesh refinement we use the method by Oden and Prudhomme [45], i.e.,

$$\text{if } \frac{|\mathcal{E}_m|}{\max_{K_m \in \mathcal{P}_h} |\mathcal{E}_m|} > \delta, \text{ then refine element } m, \quad (37)$$

where δ is the tolerance for refinement, i.e., $0 < \delta < 1$. In the following numerical verification, we pick $\delta = 0.5$. The QoI we consider is again the average of u in the upper right quadrant (see (22)). The primal problem is approximated using C^0 continuous polynomials of degree 2, whereas the dual problem is approximated using $p + 1 = 3$.

The initial mesh consists of 2 triangular elements and is too coarse to resolve the boundary layers in both primal and dual solutions leading to poor error indicators. This effect is shown in Figure 6, where the error indicators are largest in the corner of the

dual boundary layer which would result in mesh refinements at the 'wrong' location. To avoid initial mesh refinements that are poorly suited to reduce the error in the QoI, we initially perform uniform mesh refinements until the error estimate $\hat{\eta}_{est}$ begins to decrease and indicate that the error indicators ε_m (30) have become reliable.

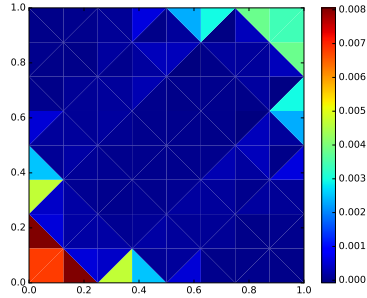


Figure 6: Element-wise distribution of the error indicators ε_m (30) on a coarse mesh.

This can for example be seen in Figure 7, where we show the solution and element-wise error indicators on a uniform mesh of 16×16 elements, the last mesh that has been uniformly refined and $\hat{\eta}_{est}$ started to decrease. Here, we see that indicators in corner of the primal boundary layer are now of a magnitude that result in local mesh refinements in the right locations. In Figure 8, we show the error indicators for an inter-

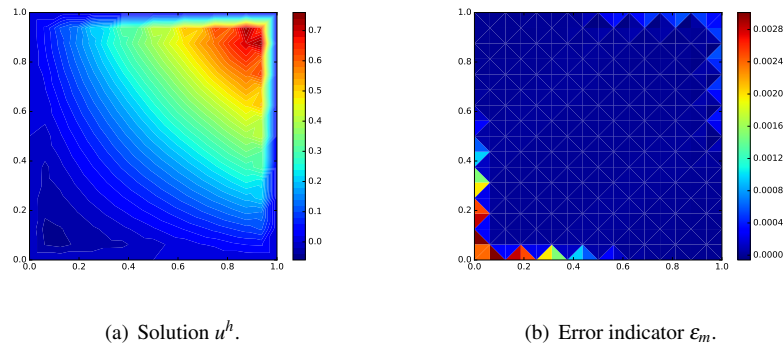


Figure 7: Solution on a uniform 16×16 mesh.

mediate (step 9) and the final (step 18) step of the adaptive process. In both cases, the mesh has been refined such that the boundary layers in both primal and dual problems

are sufficiently resolved to yield error indicators that are highest in the region of the QoI. The corresponding final adapted mesh is shown in Figure 9. As expected from the current choice of QoI, the mesh refinements have been focused near the primal boundary layer and the QoI. Lastly, we present the convergence history of the error

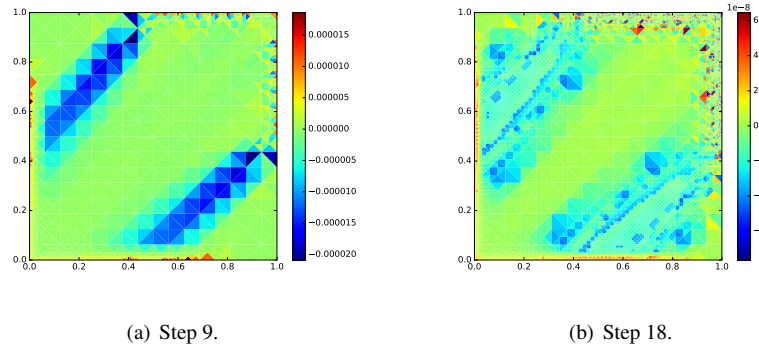


Figure 8: Error indicators ε_m .

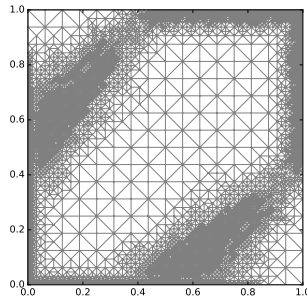


Figure 9: Final mesh of the goal-oriented h -adaptive refinements.

estimator $\hat{\eta}_{est}$ and the effectivity index $\hat{\mathcal{S}}_{eff}$ in Figure 10. The plot of estimated error and $\|u - u^h\|_{L^2(\Omega)}$ in Figure 10(a) shows that while the adaptive process ensures a small error in the QoI, the global error in the $L^2(\Omega)$ norm is several orders of magnitude larger as expected since the adaptive process is targeting to reduce the error in the QoI rather than $\|u - u^h\|_{L^2(\Omega)}$. The effectivity index shown in Figure 10(b) demonstrates that the proposed alternative approach to goal-oriented error estimation delivers highly accurate estimates even when the error becomes very small.

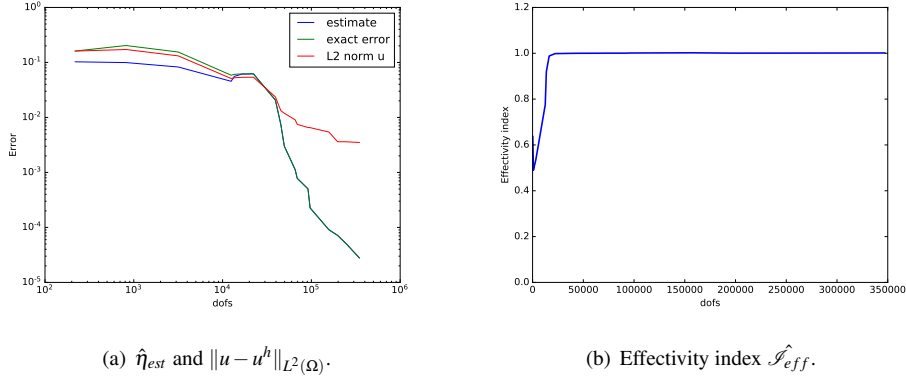


Figure 10: Convergence history for goal-oriented adaptive mesh refinement.

As a final numerical verification we consider the flux q_x across the line between $y = 0.5$ and $y = 0.75$ on the left edge of the unit square in (36), and we keep the same physical parameters as the corresponding verification, i.e., $\mathbf{b} = \{1, 1\}^T$ and $Pe = 10$. The primal problem is approximated using C^0 continuous polynomials of degree 2, whereas the dual problem is approximated using the same type polynomials at degree $p + 1 = 3$. The initial mesh consists of 512 triangle elements, we employ the adaptive strategy as in (37) with identical tolerance as well, and we perform 10 mesh refinements here. This initial mesh is chosen to be sufficiently fine to adequately resolve the boundary layers to reduce pollution effects. In Figure 11(a), the convergence history of the error indicator as well as the global L^2 error in u . The corresponding effectivity index in Figure 11(b) shows that the estimate remains highly accurate during the adaptive process. Lastly, the final adapted mesh shown in Figure 12 show that the refinements are focused near the QoI as expected for the current refinement criterion.

6. Conclusions

We have presented goal-oriented *a posteriori* error estimates for the AVS-FE method. This method is a hybrid Petrov-Galerkin method which uses classical $C^0(\Omega)$ or Raviart-Thomas FE trial basis functions, while the test space consists of functions that are discontinuous across element edges. The broken topology of the test space allows us to

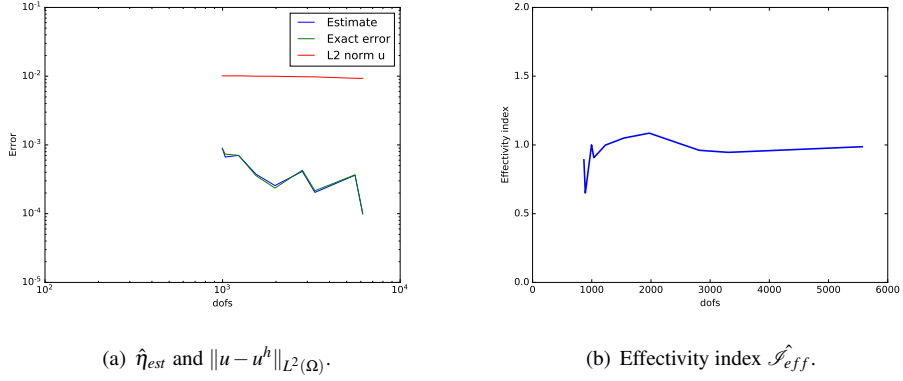


Figure 11: Convergence history for goal-oriented adaptive mesh refinement a flux QoI (36).

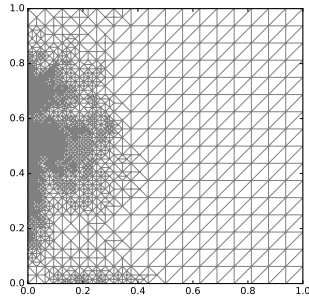


Figure 12: Final mesh of the goal-oriented h -adaptive refinements using a flux QoI (36).

employ the DPG philosophy and compute optimal test functions element-by-element, i.e., completely locally. In an effort to derive *a posteriori* error estimates of the AVS-FE computations we have introduced two types goal-oriented error estimates. The first estimate follows the classical approach of [7] where, by duality, the dual solution is sought in the test space V , which in the case of the AVS-FE method is a broken Hilbert space. However, we show that through numerical verifications of the classical Laplace BVP that this approach yields error estimates with poor accuracy. To resolve this, we introduce a second estimate based on consideration of the PDE that governs the dual solution. The estimate is then established by computing $C^0(\Omega)$ or Raviart-Thomas AVS-FE approximations of this PDE. Numerical verifications involving pure diffusion

as well as convection-dominated diffusion problems show that the new alternative error estimate is capable of accurately predicting errors for different QoIs and mesh partitions.

In order to employ the new *a posteriori* error estimation methodology in mesh adaptivity we also here derived error indicators to guide any h -adaptive process. The error indicators essentially are the element-wise restriction of the residual operator (30). Numerical verifications show that when the error indicators used with classical refinement strategies [45], they lead to a mesh adaptive process able to reduce the error in the QoI within a defined accuracy while at the same time delivering highly accurate predictions of the error in the QoI even when the error is small. In a previous paper [1], the results presented are all computed using C^0 approximations for both trial variables. Here, we also presented results in which the fluxes are computed by using Raviart-Thomas approximations. These results indicate that C^0 approximations yield results that are of the same quality in terms of both error estimation, and result in slightly higher accuracy for the flux variable at a slightly lower number of degrees of freedom. Hence, the use of C^0 approximations for both variables remains attractive due to its lower computational cost, and ease of implementation in existing FE software.

Note that the domains considered in the verifications in Section 4.2.3 are convex, it is likely that for non-convex domains the consistency of Raviart-Thomas approximations will be preferable over our C^0 approximations. This investigation is postponed to future research efforts. The poor performance of the classical method reported in Section 3 appears to be related to regularity of the dual solution as suggested by DPG* literature. Hence, in future efforts we will pursue analyses of the dual problem within a framework similar to the DPG* method to fully understand the intricacies of the dual solution.

In a forthcoming paper, we intend to extend the AVS-FE method and the new alternative error estimates to other problems such as the nonlinear Cahn-Hilliard equation, as well as alternative error indicators as proposed in, e.g., [46].

Acknowledgements

The numerical verifications presented in Section 4.2.3 were computed using the computational framework Firedrake [47] and the h -adaptive process presented in Section 5 was implemented in the computational framework FEniCS [48].

This work has been supported by the United States National Science Foundation - NSF CBET Program, under NSF Grant titled *Sustainable System for Mineral Beneficiation*, NSF Grant No. 1805550.

References

- [1] V. M. Calo, A. Romkes, E. Valseth, Automatic Variationally Stable Analysis for FE Computations: An Introduction, Lecture Notes in Computational Science and Engineering, accepted, arXiv preprint arXiv:1808.01888. (2018).
- [2] L. Demkowicz, J. Gopalakrishnan, A class of discontinuous Petrov-Galerkin methods. Part I: The transport equation, *Computer Methods in Applied Mechanics and Engineering* 199 (23) (2010) 1558–1572.
- [3] C. Carstensen, L. Demkowicz, J. Gopalakrishnan, A posteriori error control for DPG methods, *SIAM Journal on Numerical Analysis* 52 (3) (2014) 1335–1353.
- [4] L. Demkowicz, J. Gopalakrishnan, Analysis of the DPG method for the Poisson equation, *SIAM Journal on Numerical Analysis* 49 (5) (2011) 1788–1809.
- [5] L. Demkowicz, J. Gopalakrishnan, A class of discontinuous Petrov-Galerkin methods. II. Optimal test functions, *Numerical Methods for Partial Differential Equations* 27 (1) (2011) 70–105.
- [6] L. Demkowicz, J. Gopalakrishnan, A class of discontinuous Petrov-Galerkin methods. Part III: Adaptivity, *Applied numerical mathematics* 62 (4) (2012) 396–427.
- [7] R. Becker, R. Rannacher, An optimal control approach to a posteriori error estimation in finite element methods, *Acta Numerica* 10 (2001) 1–102.

- [8] M. Ainsworth, J. T. Oden, A posteriori error estimation in finite element analysis, Vol. 37, John Wiley & Sons, 2011.
- [9] J. T. Oden, L. Demkowicz, W. Rachowicz, T. Westermann, Toward a universal hp adaptive finite element strategy, part 2. a posteriori error estimation, *Computer Methods in Applied Mechanics and Engineering* 77 (1-2) (1989) 113–180.
- [10] J. T. Oden, S. Prudhomme, Estimation of modeling error in computational mechanics, *Journal of Computational Physics* 182 (2) (2002) 496 – 515.
- [11] M. B. Giles, E. Süli, Adjoint methods for PDEs: a posteriori error analysis and postprocessing by duality, *Acta numerica* 11 (2002) 145–236.
- [12] P. Ladevèze, F. Pled, L. Chamoin, New bounding techniques for goal-oriented error estimation applied to linear problems, *International journal for numerical methods in engineering* 93 (13) (2013) 1345–1380.
- [13] S. Prudhomme, J. T. Oden, On goal-oriented error estimation for elliptic problems: application to the control of pointwise errors, *Computer Methods in Applied Mechanics and Engineering* 176 (1-4) (1999) 313–331.
- [14] I. G. Bubnov, Reports on the works of professor Timoshenko which were awarded the Zhuranskyi Prize, *Collection of Works of the Engineers Institute of Putey Soobshcheniya Imperatora Alexandra I* 81 (1913) 1–40, in Russian.
- [15] G. Petrov, Application of the method of Galerkin to a problem involving the stationary flow of a viscous fluid, *Prikl. Matem. Mekh* 4 (3) (1940).
- [16] T. J. R. Hughes, *The finite element method: linear static and dynamic finite element analysis*, Dover Publications, 2012.
- [17] J. T. Oden, J. N. Reddy, *An introduction to the mathematical theory of finite elements*, Dover Publications, 2012.
- [18] J. N. Reddy, *An introduction to the finite element method*, Vol. 2, McGraw-Hill New York, 1993.

- [19] D. Kuzmin, S. Korotov, Goal-oriented a posteriori error estimates for transport problems, *Mathematics and Computers in Simulation* 80 (8) (2010) 1674–1683.
- [20] J. M. Cnossen, H. Bijl, M. I. Gerritsma, B. Koren, Aspects of goal-oriented model-error estimation in convection-diffusion problems, in: *ECCOMAS CFD 2006: Proceedings of the European Conference on Computational Fluid Dynamics*, Egmond aan Zee, The Netherlands, September 5-8, 2006, Delft University of Technology; European Community on Computational Methods, 2006.
- [21] K. Schwegler, M. P. Bruchhäuser, M. Bause, Goal-oriented a posteriori error control for nonstationary convection-dominated transport problems, *arXiv preprint arXiv:1601.06544* (2016).
- [22] L. Formaggia, S. Perotto, P. Zunino, An anisotropic a-posteriori error estimate for a convection-diffusion problem, *Computing and Visualization in Science* 4 (2) (2001) 99–104.
- [23] K. Schwegler, Adaptive goal-oriented error control for stabilized approximations of convection-dominated problems, Ph.D. thesis (2014).
- [24] A. N. Brooks, T. J. R. Hughes, Streamline upwind / Petrov-Galerkin formulations for convection dominated flows with particular emphasis on the incompressible Navier-Stokes equations, *Computer Methods in Applied Mechanics and Engineering* 32 (1982) 199–259.
- [25] I. Mozolevski, S. Prudhomme, A robust goal-oriented estimator based on the construction of equilibrated fluxes for discontinuous Galerkin finite element approximations of convection-diffusion problems, hal-01130388 (2015).
- [26] P. B. Bochev, M. D. Gunzburger, *Least-Squares Finite Element Methods*, Vol. 166, Springer Science & Business Media, 2009.
- [27] A. H. Niemi, N. O. Collier, V. M. Calo, Automatically stable discontinuous Petrov–Galerkin methods for stationary transport problems: Quasi-optimal test space norm, *Computers & Mathematics with Applications* 66 (10) (2013) 2096–2113.

- [28] B. Keith, F. Fuentes, L. Demkowicz, The DPG methodology applied to different variational formulations of linear elasticity, *Computer Methods in Applied Mechanics and Engineering* 309 (2016) 579–609.
- [29] B. Keith, A. V. Astaneh, L. F. Demkowicz, Goal-oriented adaptive mesh refinement for discontinuous petrov–galerkin methods, *SIAM Journal on Numerical Analysis* 57 (4) (2019) 1649–1676.
- [30] J. H. Chaudhry, E. C. Cyr, K. Liu, T. A. Manteuffel, L. N. Olson, L. Tang, Enhancing least-squares finite element methods through a quantity-of-interest, *SIAM Journal on Numerical Analysis* 52 (6) (2014) 3085–3105.
- [31] Z. Cai, J. Ku, Goal-oriented local a posteriori error estimators for H (div) least-squares finite element methods, *SIAM Journal on Numerical Analysis* 49 (6) (2011) 2564–2575.
- [32] J. Ku, E.-J. Park, A posteriori error estimators for the first-order least-squares finite element method, *Journal of computational and applied mathematics* 235 (1) (2010) 293–300.
- [33] J. Ku, A posteriori error estimates for the primary and dual variables for the div first-order least-squares finite element method, *Computer Methods in Applied Mechanics and Engineering* 200 (5-8) (2011) 830–836.
- [34] E. Valseth, Automatic Variationally Stable Analysis for Finite Element Computations, Ph.D. thesis (2019).
- [35] V. Girault, P.-A. Raviart, Finite element methods for Navier-Stokes equations; theory and algorithms, in: *Springer Series in Computational Mathematics*, Vol. 5, Springer-Verlag, 1986.
- [36] I. Babuška, Error-bounds for finite element method, *Numerische Mathematik* 16 (1971) 322–333.
- [37] C. Carstensen, L. Demkowicz, J. Gopalakrishnan, Breaking spaces and forms for the DPG method and applications including maxwell equations, *Computers & Mathematics with Applications* 72 (3) (2016) 494–522.

- [38] B. Keith, S. Petrides, F. Fuentes, L. Demkowicz, Discrete least-squares finite element methods, *Computer Methods in Applied Mechanics and Engineering* 327 (2017) 226–255.
- [39] S. Nagaraj, S. Petrides, L. F. Demkowicz, Construction of DPG Fortin operators for second order problems, *Computers & Mathematics with Applications* 74 (8) (2017) 1964–1980.
- [40] S. Prudhomme, J. T. Oden, Computable error estimators and adaptive techniques for fluid flow problems, in: *Error estimation and adaptive discretization methods in computational fluid dynamics*, Springer, 2003, pp. 207–268.
- [41] L. Demkowicz, J. Gopalakrishnan, B. Keith, The DPG-star method, *Computers & Mathematics with Applications* (2020).
- [42] J. A. Bramwell, A discontinuous Petrov–Galerkin method for seismic tomography problems (2013).
- [43] P. A. Raviart, J. M. Thomas, *A Mixed Finite Element Method For Second Order Elliptic Problems*, Springer, 1977.
- [44] F. Brezzi, M. Fortin, *Mixed and Hybrid Finite Element Methods*, Vol. 15, Springer-Verlag, 1991.
- [45] J. T. Oden, S. Prudhomme, Goal-oriented error estimation and adaptivity for the finite element method, *Computers and Mathematics with Applications* 41 (5-6) (2001) 735–756.
- [46] V. Darrigrand, Á. Rodríguez-Rozas, I. Muga, D. Pardo, A. Romkes, S. Prudhomme, Goal-oriented adaptivity using unconventional error representations for the multidimensional helmholtz equation, *International Journal for Numerical Methods in Engineering* 113 (1) (2018) 22–42.
- [47] F. Rathgeber, D. A. Ham, L. Mitchell, M. Lange, F. Luporini, A. T. McRae, G.-T. Bercea, G. R. Markall, P. H. Kelly, *Firedrake: automating the finite element*

method by composing abstractions, *ACM Transactions on Mathematical Software (TOMS)* 43 (3) (2017) 24.

- [48] M. S. Alnæs, J. Blechta, J. Hake, A. Johansson, B. Kehlet, A. Logg, C. Richardson, J. Ring, M. E. Rognes, G. N. Wells, The fenics project version 1.5, *Archive of Numerical Software* 3 (100) (2015) 9–23.